 doi:10.20944/preprints202008.0037.v2

Article

Effect of pH on the formation of amorphous TiO_2 complexes and TiO_2 anatase during pyrolysis of aqueous $TiCl_4$ solution

Mai Van Tuan [1,2], Mai Xuan Dung [3], and Duong Ngoc Huyen [1,*]

[1] School of Engineering Physics, Hanoi University of Science and Technology, No. 1, Daicoviet, Hanoi, Vietnam; huyen.duongngoc@hust.edu.vn
[2] Department of Natural Sciences, Electric Power University, 235 Hoang Quoc Viet, Hanoi, Viet Nam; tuanmvns@gmail.com
[3] Department of Chemistry, Hanoi Pedagogical University 2, 32 Nguyen Van Linh, Phuc Yen, Vinh Phuc, Viet Nam; xdmai@hpu2.edu.vn
* Correspondence: huyen.duongngoc@hust.edu.vn; Tel.: +84-912 153 128

Abstract: The TiO_2 nanostructures resulted by pyrolysis of $TiCl_4$ at low temperature of 80 ^oC are found to be a mixture of amorphous TiO_2 complexes and anatase nanostructure whose ratio depends on the pH of the pyrolysis medium. At low pH level, the resulting TiO_2 nanostructure is predominant anatase and gradually shifts to the amorphous TiO_2 complexes with pH level increasing. By means of heat treatment, the amorphous TiO_2 complexes can be converted back to the anatase nanostructure and then transform to rutile with the elevating temperature. Amongst of the TiO_2 nanostructure recovered from amorphous TiO_2 complexes, the anatase shows to be the most effective photocatalyst in decomposition of methylene blue.

Keywords: photocatalyst, amorphous TiO_2 complexes, TiO_2, anatase nanostructure.

1. Introduction

Titanium dioxide (TiO_2), a typical metal oxide with high refractive index, chemical stability, long durability, and nontoxicity has been widely used for many applications such as white pigments, textiles, papers, cosmetics, medicines, ceramics, etc. As a *n*-type wide bandgap semiconductor, TiO_2 exhibits a unique photoinduced effect that involves photogenerated charge carriers on the material surface that initiate strong redox reaction of adsorbed substances and hydrophilic conversion of itself [1, 2]. The effect offers more potential applications involving photochemical processes such as splitting hydrogen from water, photocatalyst, photoconductor, environment cleaning, antibacterial purpose, chemical sensors, ultraviolet fillers, dye-sensitized solar cells (DSSC) and so forth [3 - 5].

Under normal condition, TiO_2 exists in three main structures: stable rutile, metastable anatase, and brookite phase. For pure phase it is generally accepted that anatase exhibits a higher photocatalytic activity compared to that of rutile despite of its larger band gap (3.2 eV for anatase vs. 3.0 eV for rutile). Longer lifetime for photo-excited electrons and holes in the indirect band gap of TiO_2 anatase semiconductor is accounted for the feature [6]. On the other hand, TiO_2 in the microstructure have been considered as a poor photocatalyst but in the nanostructured form, due to the quantum confinement the material shows stronger photocatalytic activity in comparison to that of the microstructure [7]. The unique photocatalyst of TiO_2 is size and structure dependent. Therefore, clarification out the synthesis conditions to achieve desirable nanostructures of TiO_2 is of important to diverse photocatalystic applications.

Preprints (www.preprints.org) | NOT PEER-REVIEWED | Posted: 7 September 2020 doi:10.20944/preprints202008.0037.v2

With regard to the synthesis of TiO_2 nanostructure, a variety of techniques based on pyrolysis of Ti precursors such as hydrothermal, solvothermal, sol-gel, direct oxidation, chemical vapor deposition (CVD), electrodeposition, sonochemical, and microwave method has been used [8]. Pyrolysis offers a simple route to synthesize well-crystalline TiO_2 using inexpensive precursors such as titanium (IV) tetrachloride $TiCl_4$, titanium (IV) butoxide, titanium(IV) isopropoxide, amorphous TiO_2, P_{25}, etc. In addition, the pyrolysis modest medium of low temperature and adjustable pyrolysis time can provide an effective environment for the synthesis of TiO_2 with high purity, good dispersion and controllable crystalline. From the viewpoint of chemical thermodynamics, before decomposing into TiO_2 either in the form of anatase, brookite or rutile, the titanium precursor undergoes a series of amorphous TiO_2 complexes (or intermediates) such as $Ti_xO_yCl_z(OH)_w$ resulting from pyrolysis of $TiCl_4$, $[Ti(OH)_{4-n}(H_2O)_{2+n}]^{n+}$ from Ti(IV)-butoxide or $[Ti_{3(y+1)}O_{4y}(OBu)_{4(y+3)-x}(OEt)_x]$ from alkoxide metal $M(OR)_n$ [9-11]. Hence, the amorphous TiO_2 complexes also can be used as a kind of secondary precursor to produce desirable brookite, anatase, or rutile structure [12]. Elucidation out of the formation and conversion of amorphous TiO_2 complexes is assumed to be a critical point to synthesize and bring in desirable TiO_2 nanostructures. With respect to the amorphous $Ti_xO_yCl_z(OH)_w$ complexes resulted from pyrolysis of $TiCl_4$, the substitution of OH for Cl radicals in the complexes does not lead to much change in the core involving the Ti atoms but a difference in bond lengths and potential energy surfaces [9]. Change relative ratio of the Cl and OH radicals then is considered to be an effective approach to control the complex intermediates and realize the final desirable TiO_2 nanostructures. For example, an increase of the Cl radical in the pyrolysis medium by addition of HCl or higher $TiCl_4$ concentration has shown to promote the formation of the brookite and rutile structure [13, 14]. In an experiment made on pyrolysis of aqueous $TiCl_4$ solution with HCl additive, we have found that a nanocrystalline mixture of both the anatase and rutile phase is resulted. The TiO_2 anatase mainly suspends in the aqueous solution while the TiO_2 rutile predominantly deposits in the sedimentation [15, 16]. Higher HCl concentration enables the agglomeration of anatase particles and enhances the anatase to rutile transition due to the compensation of Cl radical for the positive charge of polyhedral complexes [15]. On the other hand, an increase of the OH radical in the $TiCl_4$ pyrolysis medium by addition of a basic agent such as NH_4OH is expected to give the additional modification on the complexes. Based on those considerations, in this study an experiment is carried on to investigate the effect of pH level (or OH radical) on the formation of amorphous TiO_2 complexes as well as of final anatase nanostructure resulting from pyrolysis of aqueous $TiCl_4$ solution.

2. Results and Discussion

Experiments show that the additive NH_4OH significantly affects the appearance and properties of TiO_2 nanostructures in the resulting materials. As clearly seen in Figure 1, the resulting aqueous solution appears transparent at low pH level but gradually changes to slightly opalescent and then separates into transparent and milky parts when the pH level exceeding 2.40. The separated milky column increases with NH_4OH and becomes unchanged as pH level exceeding 7.34. Depending on the transparent or milky state, the surface morphology of the resulting materials transforms from grain to gelation structure as shown in the SEM images in Figure 2. In the sample with pH of 0.98, the resulting material grains are uniform granular with mean size of around 50-70 *nm*, that in turn has found to be clusters of anatase nanoparticles of 4-5 nm in the mean size [15]. However, when the pH level of the reactive medium increases, the resulting material grain increasingly inflates to coagulated clusters of 150-200 nm in size and gradually become jellylike or amorphous as shown in Fig. 2b to Fig. 2d.

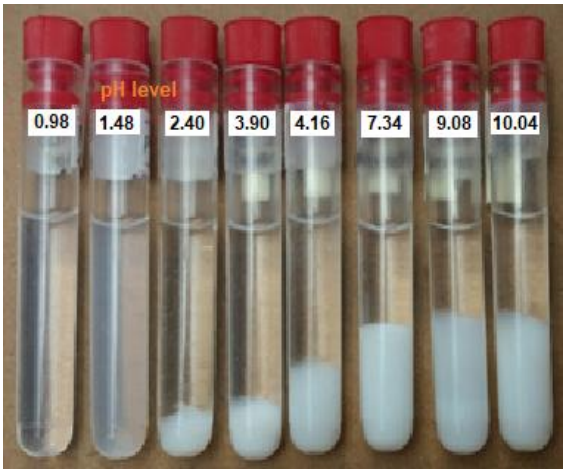

Figure 1. The appearance of aqueous $TiCl_4$ solution with different pH level after pyrolysis at 80 °C.

Preprints (www.preprints.org) | NOT PEER-REVIEWED | Posted: 7 September 2020 doi:10.20944/preprints202008.0037.v2

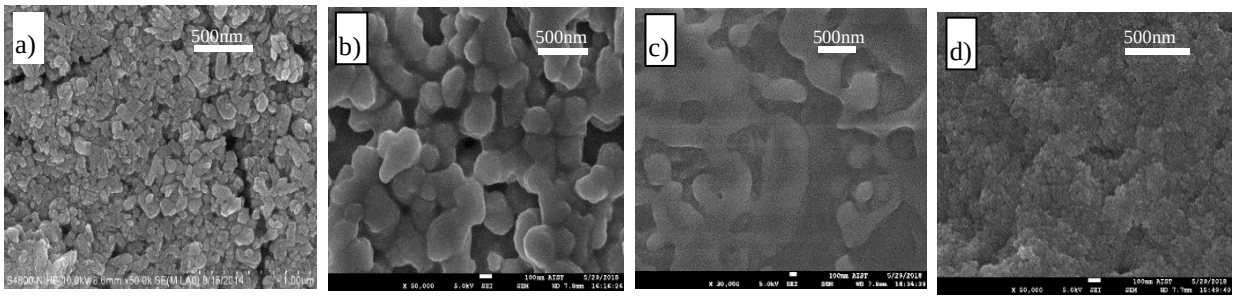

Figure 2. SEM images of TiO_2 resulting from pyrolysis of $TiCl_4$ in different pH medium at 80 °C: (a) pH = 0.98; (b) pH = 2.45; (c) pH = 10.0 transparent part; (d) pH = 10.0 milky part.

X-ray diffraction spectra in Figure 3 show the evolution of the resulting materials depending on the pH level, i.e, on NH_4OH additive. In the sample with pH level of 0.98, the XRD pattern contains principal peak around 25.29° and the other peaks around 37.80°, 48.05°, 53.89°, 62.68° respectively asigning for the diffraction of anatase structure at (101) and (004), (200), (105), (204) planes (JCPDS no. 00-021-1272). When NH_4OH is added, together with the diffraction peaks from anatase the other sharp diffraction peaks at 22,98°, 32,69°, 40,31°, 46,88°, 52.80°, 58.29°, 68.43° standing for the diffractions at (100), (110), (111), (200), (210), (211), and (220) planes, respectively from NH_4Cl crystal [17] are emerged. With the increase of pH level as NH_4OH additive increaing, the TiO_2 diffraction in the XRD pattern is gradually desapeared. The gradual disappearance of TiO_2 diffraction in XRD pattern is account for the gradual conversion from TiO_2 anatase to amorphous TiO_2 complexes. Using Scherrer equation, i.e., $D = k\lambda/\beta\cos\theta$, where k = 0.94, λ = 0.154 nm and β is FWHM at diffraction angle θ according to (101) peak to calculate the mean size D of anatase particles, it has found that the mean sizes of anatase particle is almost unchanged around 4.5 nm as given in Table 1. This value is considered to be the limitation of anatase size in the conversion to amorphous TiO_2 complexes.

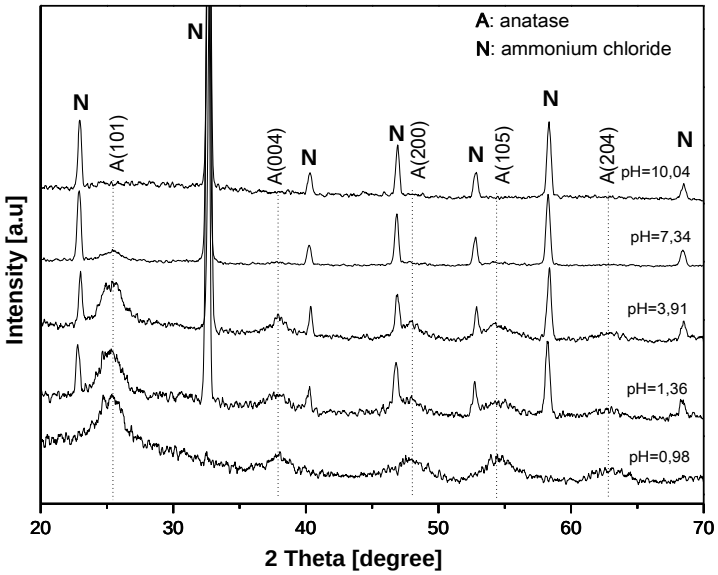

Figure 3. XRD spectra of TiO_2 resulting from pyrolysis of $TiCl_4$ in different pH medium at 80 °C.

Table.1. The mean size of anatase particle rsulted from pyrolysis of $TiCl_4$ in different pH medium at 80 °C.

pH	(101) peak FWHM	Size (nm)	Agent addition
0.98	2,007	4,3	No addition
1,36	1,889	4,5	NH_4OH
3,91	1,830	4,7	NH_4OH
7,34	1,888	4,5	NH_4OH
10.04	-	-	NH_4OH

Preprints (www.preprints.org) | NOT PEER-REVIEWED | Posted: 7 September 2020 doi:10.20944/preprints202008.0037.v2

Raman spectra also confirm the presence of anatase and NH_4Cl in the resulting materials. As shown in Figure 4, in the starting materials, namely, the sample with pH level of 0,98, the spectrum exhibits vibrational mode around 155 cm^{-1}, 399 cm^{-1}, 513 cm^{-1} and 634 cm^{-1} respectively representing the E_g, B_{1g}, $A_{1g} + B_{1g}$ and E_g modes of anatase structure [18]. The presence of NH_4Cl in the materials gives rise to a broad saddle spectrum consisting of two vibration modes around 168 cm^{-1} and 144 cm^{-1} that is asumed to be the supposition of E_g vibration mode of anatase and ν_2, ν_3 and ν_4 vibration modes of NH_4Cl oscilating against Cl along (100) direction and along three orthogonal directions [20].

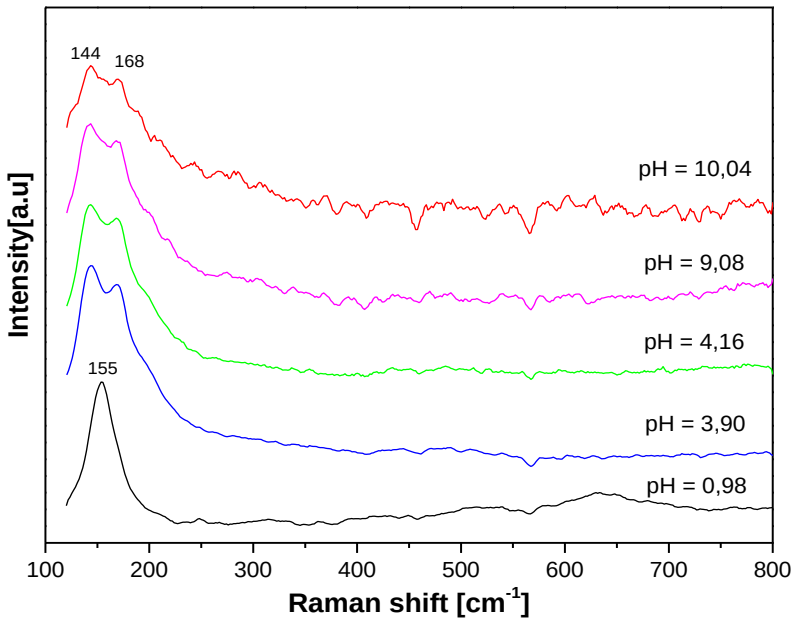

Figure 4. Raman spectra of TiO_2 resulting from pyrolysis of $TiCl_4$ in different pH medium at 80 °C.

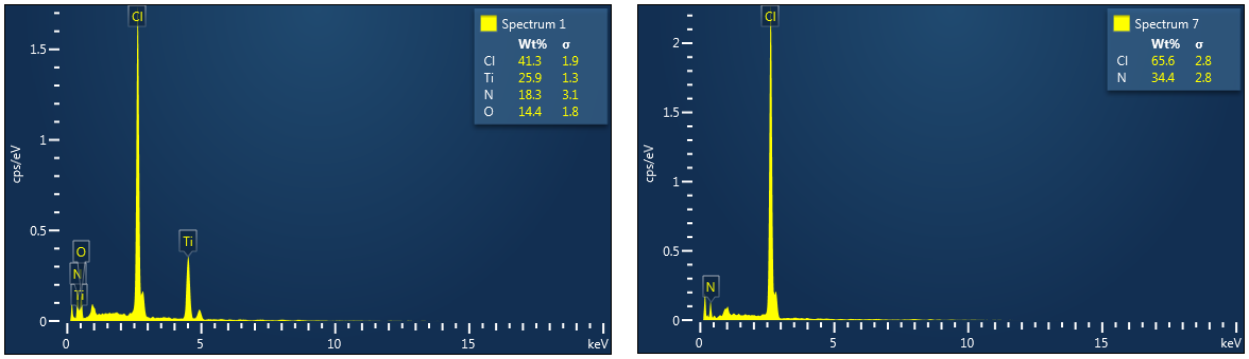

a) b)

Figure 5. EDS spectra of sample extracted from the milky part **a**) and from the transparent part **b**) that is extracted from pyrolysis of $TiCl_4$ in a medium with pH = 10.04.

The appearance of transparent, opalescent and separable milky part in the solution is believed to be due to the appearance and increase of amorphous TiO_2 complexes forming in the pyrolysis medium. At low pH level, in the acidic aqueous medium with higher concentration of hydrogen ions the formation of amorphous TiO_2 complexes is negligible, the resulting anatase is crystallized in the form of grain structure with sharp boundary. The presence of NH_4OH in the pyrolysis medium will raise the pH level anh then the OH radical that promotes the formation of amorphous TiO_2 complexes. Consequently, with the increase in NH_4OH additive, the separated milky fraction in the medium is gradually increased in agreement with the gradual decrease of anatase diffraction in the XRD spectra. When the pH level exceeding 7.34, the milky column is unchanged even though the NH_4OH additive keeps increasing. Furthermore, the EDS spectra show that no trace of Ti presents in the transparent but in the milky part as given in Figure 5. This indirectly indicates that the decomposed $TiCl_4$ precusor is totally converted into

Preprints (www.preprints.org) | NOT PEER-REVIEWED | Posted: 7 September 2020 doi:10.20944/preprints202008.0037.v2

amorphous TiO_2 complexes as the pH level exceeding 7.34. Due to the armophous nature, no diffraction partten of amorphous TiO_2 complexes is observed in XRD spectra as pH level beyond that point.

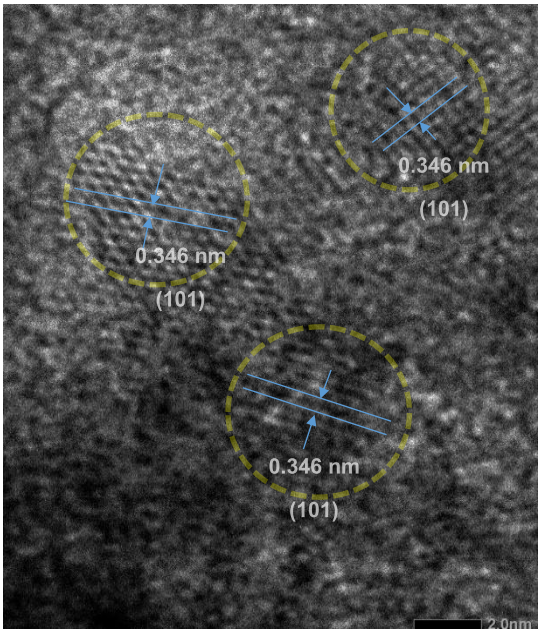

Figure 6. The appearance of anatase nanoparticle scatteringly embedded in the amorphous TiO_2 complexes.

HRTEM image taken from milky sample with pH level of 10.04 as given in Figure 6 shows the appearance of tiny nanocrystallites scatteringly embedded in an amorphous medium. The amorphous medium surrounding materials is considered to be the amorphous TiO_2 complexes. A lattice spacing of the tiny nanocrystallite around 0.346 nm is identical as the lattice spacing of the (101) plane of TiO_2 anatase. The estimated size of TiO_2 anatase particle is comparable to those calculated from XRD pattern, around 4.5 nm that is considered to be the size limitation of anatase in equilibrium with amorphous TiO_2 complexes. The presence of anatase nanoparticles embedded in the amorphous TiO_2 complexes elucidates for the appearance of E_g vibration mode of anatase in Raman spectra in Figure 4.

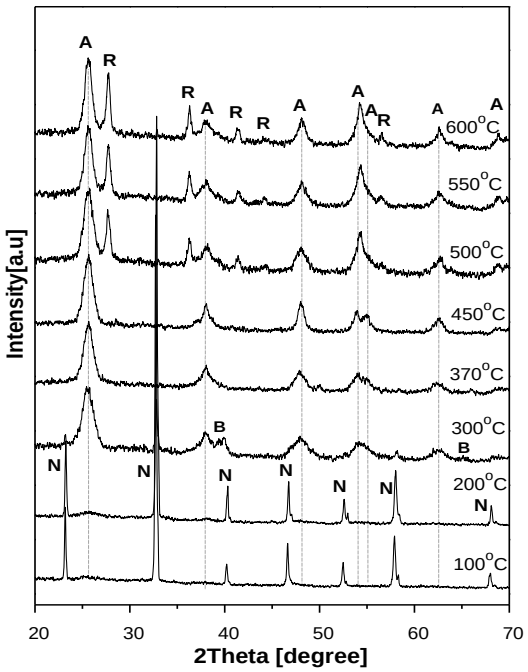

Figure 7. XRD spectra of TiO_2 that resulted from pyrolysis of $TiCl_4$ in the medium with pH =10.04 at 80 °C and then are treated in different elevated temperature, A (anatase), B (brookite), R (rutile), N (ammonium chloride).

Preprints (www.preprints.org) | NOT PEER-REVIEWED | Posted: 7 September 2020 doi:10.20944/preprints202008.0037.v2

Under heat treatment at elevated temperature, the XRD and Raman spectra demontrate the conversion from amorphous TiO_2 complexes back to anatase and then from anatase to rutile. At heating temperature bellow 200 °C, the XRD pattern in Figure 7 shows only the trace of NH_4Cl but not anatase nor brookite nor rutile. However, when heating temperature exceeds 200 °C the anatase diffraction is gradually emerging while NH_4Cl diffraction is gradually disappearing in the XRD patterns. The disapearance of NH_4Cl is accounted for the decomposition of the materials into NH_3 and HCl gases while the apearance TiO_2 anatase is explianed fro the decomposition and recrystallination of amorphous TiO_2 complexes at elevated temperature. When the heating temperature exceeds 300 °C, the NH_4Cl is completely decomposed and the complexes is totally converted into TiO_2 nanostructure with predominant anatase. The brookite and rutile structure are hardy observed in the XRD patterns and can be negleted in the conversion process. When the heating temperature exceeds 450 °C the appearance of rutile diffraction in the XRD patterns indicates the onset of the anatase-ruttile transition. The mean size of anatase calculated from XRD patterns is found to grow from around 4.5 nm at heating temperature of 200 °C to 8.9 nm at heating temperature of 600 °C as given in Table 2. For the sample with pH level of 0.98, the anatase is predominant over amorphous TiO_2 complexes, the heat treatment is merely the mean to enable the separation of the anatase nanoparticle from the cluster.

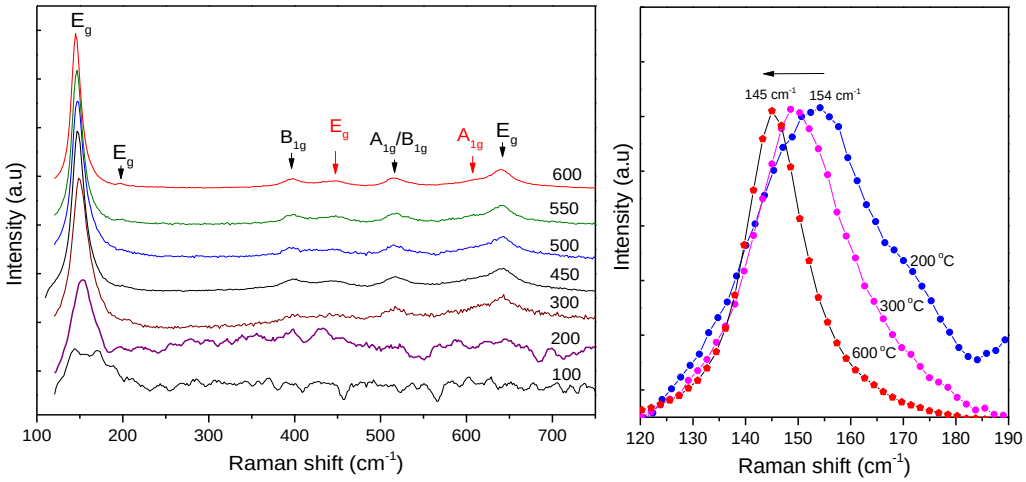

Figure 8. (a) Raman spectra of TiO_2 that resulted from pyrolysis of $TiCl_4$ in the medium with pH = 10.04 at 80 °C and then are treated in different temperature; (b) blue shift of E_g vibration mode as the heating temperature increases from 200 °C to 600 °C.

The Raman spectra also verify the conversion of anatase from the amorphous TiO_2 complexes (the milky part) when it is heat up as given in Figure 8. With baking temperature bellow 200 °C the Raman spectrum is a composition of NH_4Cl vibration mode centered around 168 cm^{-1} and 144 cm^{-1} and the Eg vibration mode of TiO_2 anatase at 147 cm^{-1}. As the heating temperature increases from 200 °C to 600 °C the E_g vibration mode shows a shift in frequency from 154 cm^{-1} to 145 cm^{-1} and a shrinkage in FWHM (see in Table 2). The feature accounts for the size growth from 4.5 nm to 8.9 nm of the TiO_2 anatase nanocrystallites [18].

The formation of TiO_2 nanostructures by pyrolysis of $TiCl_4$ in elevated pH medium can be explained by the decomposition, dissolution mechanism [20]. At elevated temperature exceeding 80 °C, $TiCl_4$ is decomposed into HCl and amorphous $Ti_xO_yCl_z$ (or $Ti_xO_yCl_z(OH)_w$) complexes and then converted into TiO_2 anatase nanostructure. The component ratio of the amorphous TiO_2 complexes and TiO_2 anatase is established by an equilibrium balance between H, OH and Cl radical concentration in the medium. At low pH level, the Cl radiacal promote the formation of anatase nanocrystallites whose mean size bellow the limitation for the anatase to rutile transition [15, 16]. On the other hand, at high pH level the presence of OH and NH_4 radical eliminates the activity of Cl radical and brings in a consequent materials of OH dominant amorphous $Ti_xO_y(OH)_w$ or $[Ti(OH)_{4-n}(H_2O)_{2+n}]^{n+}$ complexes. As a result, at low pH level the anatase fraction is dominant while the amorphous TiO_2 complexes is

Preprints (www.preprints.org) | NOT PEER-REVIEWED | Posted: 7 September 2020 doi:10.20944/preprints202008.0037.v2

dominant at high pH level. The amorphous TiO_2 complexes can be converted back to the TiO_2 anatase nanoparticles by heat treatment at elevated temperature around 300 °C.

Table.2. The mean size and Eg vibration mode of anatase resulting from annealing amorphous TiO_2 complexes.

Baking temp.	Crystallite size (nm)	E_g mode peak (cm^{-1})	FWHM of E_g mode (cm^{-1})
200°C	4.5	154	31
300°C	6.2	150	25.8
450°C	6.8	148	18.9
500°C	6.8	148	18.1
550°C	8.3	147	15.9
600°C	8.9	145	14.5

Experiments show that amorphous TiO_2 complexes and TiO_2 anatase nanoparticles exhibit strong photocatalytic activity upon exposure to UV light radiation. Quatitatively, a mixture of 50 *ml* of 0.25 *μmol* methylene blue (MB) aqueous solution and 50.0 *mg* of amorphous TiO_2 complexes or TiO_2 anatase nanoparticles is stirred magnetically under dark conditions for 30 min before exposed upon a UV mercury vapor lamp. After a fixed UV exposure duration, 1.0 *ml* of the aqueous solution is taken out for UV-Vis characterization. By comparison of the relative intensity of MB principal adsorption peak in the UV-Vis spectrum, the percentage of oxidated MB in the solution is deduced and then the photocatalytic activity of the materials is calculated.

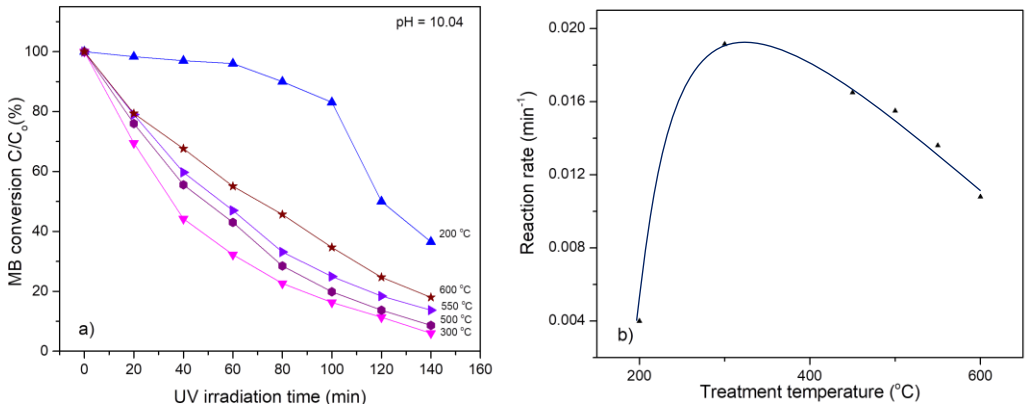

Figure 9. a) Rates of photocatalytic oxidation of MB as a function of TiO_2 complexes treated in different heating temperature ; b) Photocatalytic activity of amorphous TiO_2 complexes depends on heating temperature.

With respect to the amorphous TiO_2 complexes, the photocatalytic activity of the materials is shown to be dependent to the heating temperature. As illuminated in Figure 9a, the rates of photocatalytic oxidation of MB show to be exponential reduction that is well fitted to the Langmuir–Hinshelwood (L-H) kinetics model [22]. When MB concentration is small the L-H equation can be simplified to an apparent first-order: $ln(C_0/C_t) = kt$ or $C_t = C_0\ exp\ (-kt)$, where C_0 is the initial concentration of MB, C_t is the concentration of the MB at illumination time t, k is a constant standing for the photoctalitic redox or reaction rate. By fitting the MB decomposition curve in Figure 9 a) to the L-H equation the dependence of the photocatalytic activity of amorphous TiO_2 complexes on the heating temperature is shown in Figure 9 b). As can be seen from Fig. 9b, the photocatalystic activity (reaction rate) of the materials is weak as heating temperature bellow ~200 °C but rapid increases with elevated temperature then has the maximum at the heating temperature of around 300 °C. Further increasing

 doi:10.20944/preprints202008.0037.v2

the heating temperature, the photocatalytic activity of the materials is declined. The evaporation then elimination of NH_4Cl and the decomposition of amorphous TiO_2 complexes with the following recrystallization into anatase nanostructure in the materials is accounted for the behavior. At heating temperature around 300 °C, NH_4Cl and amorphous TiO_2 complexes are asumed to be totally decomposed the materials completely turn into pure anatase the materials exhibits the maximum photocatalytic activity. Futher increasing the heat temperature, the photocatalytic activity is reduced due to the growth in size of anatase particle and the appearance rutile fraction from the anatase-rutile transition.

3. Materials and Methods

Titanium tetrachloride ($TiCl_4$) of 99.9 % purity (Sigma Aldrich Chemical Co.) as Ti precursor was used as received. Ammonium hydroxide solution (NH_4OH) of 28 % NH_3 (Merck Corp.,) was used as basic agent to change the pH of pyrolysis medium. The TiO_2 synthesis process was straightforward as follows: $TiCl_4$ was added dropwise into DI water at 5 **°C** to a concentration of 0.04 M, the pH level of the solution then was dropped to around 0.98 (starting point). By adding a small amount of NH_4OH into the solution the pH level was adjusted and preserved at a point in range of 0.98 to 10.04. The solution then was poured into test tubes and placed in an oven at 80 **°C**, the onset point of $TiCl_4$ decomposition. The solution was gradually changed to opalescent suspension indicating that the $TiCl_4$ was thermally decomposed and converted into Ti complexes and then TiO_2 accompanying with the formation of HCl and NH_4Cl [11]. The pyrolysis was carried on about 3.0 h then the power was shut down, the solution was slowly cooled to room temperature. Depending on pH level, the appearance of resulting solution shows either transparent, opalescent or clearly splits into transparent and milky part as seen in Figure 1. For characterization, these parts were separated and dried by vacuum evaporation then were thermally treated in an oven with baking temperature up to 600 °C.

The structure of the resulting materials was determined by D8 Advance Bruker diffractometer using CuK_α radiation of 0.154 *nm* wavelength. The mean size, D of TiO_2 crystallites was calculated using Scherrer equation, i.e., $D = k\lambda/\beta\cos\theta$, where $k = 0.94$, $\lambda = 0.154$ *nm* and β is full width at half maximum (FWHM) according to the principal diffracted angle θ, i.e., (101) peak for anatase. Raman spectra were obtained on a LabRAM HR800 (Horiba) using a 632.8 nm excitation laser at a resolution of 1.0 cm^{-1}. TEM images were obtained using a JEOL JEM-2100 Transmission Electron Microscope. SEM images were conducted on a JEOL JEM-7600F Field Emission Scanning Electron Microscope. The photocatalystic activity of TiO_2 nanostrutures was determined by measuring the degradation rate of methylene blue (MB) under UV light radiation.

4. Conclusion

The pyrolysis of aqueous $TiCl_4$ solution generally results in a mixture of anatase nanostructure and amorphous TiO_2 complexes. The ratio of TiO_2 anatase nanostructure and amorphous TiO_2 complexes can be controlled by changing the pH of the pyrolysis medium. The anatase fraction is predominant at low pH level and gradually declines and completely converts to the amorphous TiO_2 complexes at high pH level. By addition of NH_4OH to adjust the pH, the pyrolysis of a 0.04M aqueous $TiCl_4$ solution results in a mixture of TiO_2 anatase nanostructure and amorphous TiO_2 complexes at pH bellow 7.34 and predominant amorphous TiO_2 beyond that point.

The amorphous TiO_2 complexes is found to be converted to TiO_2 nanostructure by heat treatment. With annealing temperature around 300 °C, the amorphous TiO_2 is completely converted into anatase nanostructure and gradually transform into rutile at high temperature. Amongst of the TiO_2 nanostructures recovered from amorphous TiO_2 complexes, the anatase nanostructure shows to be the most effective photocatalyst in decomposition of methylene blue.

Acknowledgments: The authors gratefully acknowledge financial support received in the form of a Basic Research Project Grant in Aid (T2008-PC-123) provided by Hanoi University of Science and Technology (HUST), Vietnam.

Conflicts of Interest: The authors declare no conflict of interest.

References

1. U. Diebold, The surface science of titanium dioxide, Surf. Sci. Rep. **2003**, 48, pp.53-229.
2. K. Hashimoto, H. Irie, and A. Fujishima, TiO_2 photocatalysis: a historical overview and future prospects, Jpn. J. Appl. Phys. **2005**, vol. 44 (12), pp. 8269–8285.
3. K. Nakata and A. Fujishima, TiO_2 photocatalysis: design and applications, J. Photochem. Photobiol. C **2012**, vol. 13 (3), pp. 169–189.
4. M. Montazer, S. Seifollahzadeh, Enhanced self-cleaning, antibacterial and UV protection properties of nano TiO_2 treated textile through enzymatic pretreatment. Photochem Photobiol. **2011**, 87, pp. 877–883.
5. A. Fujishima and K. Honda, Electrochemical photolysis of water at a semiconductor electrode, Nature **1972**, vol. 238 (5358), pp. 37–38.
6. L. Liu, H. Zhao, J. M. Andino & Y. Li, Photocatalytic CO_2 reduction with H_2O on TiO_2 nanocrystals: Comparison of anatase, rutile, and brookite polymorphs and exploration of surface chemistry. ACS Catal. **2012**, 2, pp. 1817–1828.
7. S. M. Gupta and M. Tripathi, A review of TiO_2 nanoparticles, Chinese Sci. Bull. **2011**, vol. 56 (16), pp. 1639–1657.
8. M. M. Byranvand, A. Nemati Kharat, L. Fatholahi, and Z. Malekshahi Beiranvand, A review on synthesis of nano-TiO_2 via different methods, J. Nanostruct., **2013**, vol. 3, pp. 1–9.
9. T. H. Wang, A. M. Navarrete-Lo´pez, S. Li, and D. A. Dixon, Hydrolysis of $TiCl_4$: Initial Steps in the Production of TiO_2, J. Phys. Chem. A **2010**, 114, 7561–7570.
10. M. A. Vargas, J. E. Rodríguez-Páez, Amorphous TiO_2 nanoparticles: Synthesis and antibacterial capacity, J. Non-Cryst Solids **2017**, 459, pp. 192–205.
11. V. Jordan, U. Javornik, J. Plavec, *et al.* Self-assembly of multilevel branched rutile-type TiO_2 structures via oriented lateral and twin attachment. Sci Rep **2016**, 6, 24216.
12. Abdullah M. Alotaibi, Sanjayan Sathasivam, *et al*, Chemical Vapor Deposition of Photocatalytically Active Pure Brookite TiO_2 Thin Films, Chem. Mater. **2018**, 30, 1353−1361.
13. J. H. Lee, and Y. S. Yang, Effect of HCl concentration and reaction time on the change in the crystalline state of TiO_2 prepared from aqueous $TiCl_4$ solution by precipitation, J. Eur. Ceram., **2005**, 25, 3573–3578,
14. S. W. Lee, K. S. Ahn, K. Zhu, N. R. Neale, and A. J. Frank, Effects of $TiCl_4$ Treatment of Nanoporous TiO_2 Films on Morphology, Light Harvesting, and Charge-Carrier Dynamics in Dye-Sensitized Solar Cells, J. Phys. Chem. C **2012**, 116, 21285−2129
15. N. T. Tung, D. Ng. Huyen, Effect of HCl on the Formation of TiO_2 Nanocrystallites, J. Nanomater. **2016**, vol. 2016, Article ID 6547271.
16. N. T. Tung, M. X. Dung and D. Ng. Huyen, Simultaneous Synthesis of Anatase Colloidal and Multiple-branched Rutile TiO_2 Nanostructures, B. Korean Chem. Soc., **2017**, 38(3); p. 401-405.
17. Downs, R. T., Bartelmehs, K. L., Gibbs, G. V., & Boisen, M. B., Interactive software for calculating and displaying X-ray or neutron powder diffractometer patterns of crystalline materials. Am. Mineral., **1993**, 78(9-10), pp. 1104-1107.
18. W. F. Zhang, Y. L. He, M. S. Zhang, Z. Yin and Q. Chen, Raman scattering study on anatase TiO2 nanocrystals, J. Phys. D: Appl. Phys. 2000, 33, pp. 912–916
19. M.N. Iliev, V.G. Hadjiev, A.P. Litvinchuk, Raman and infrared spectra of brookite (TiO_2): Experiment and theory, Vib. Spectrosc., **2013**, 64, pp. 148–152. .
20. R. S. Krishnan, Raman spectrum of ammonium chloride and its variation with temperature, Proc. Indian Acad. Sci., **1947**, A, 26 (6), 432-449.
21. S. Dai, Y. Wu, T. Sakai, Z. Du, H. Sakai, and M. Abe, Preparation of highly crystalline TiO_2 nanostructures by acid-assisted hydrothermal treatment of hexagonal-structured nanocrystalline titania/cetyltrimethy-ammonium bromide nanoskeleton, Nanoscale Res. Lett. **2010**, vol. 5(11), pp. 1829–1835,
22. G. W. Roberts and C. N. Satterfield, Effectiveness Factor for Porous Catalysts. Langmuir-Hinshelwood Kinetic Expressions, Ind. Eng. Chem. Fundamen., **1965**, 4, 3, pp. 288–293.